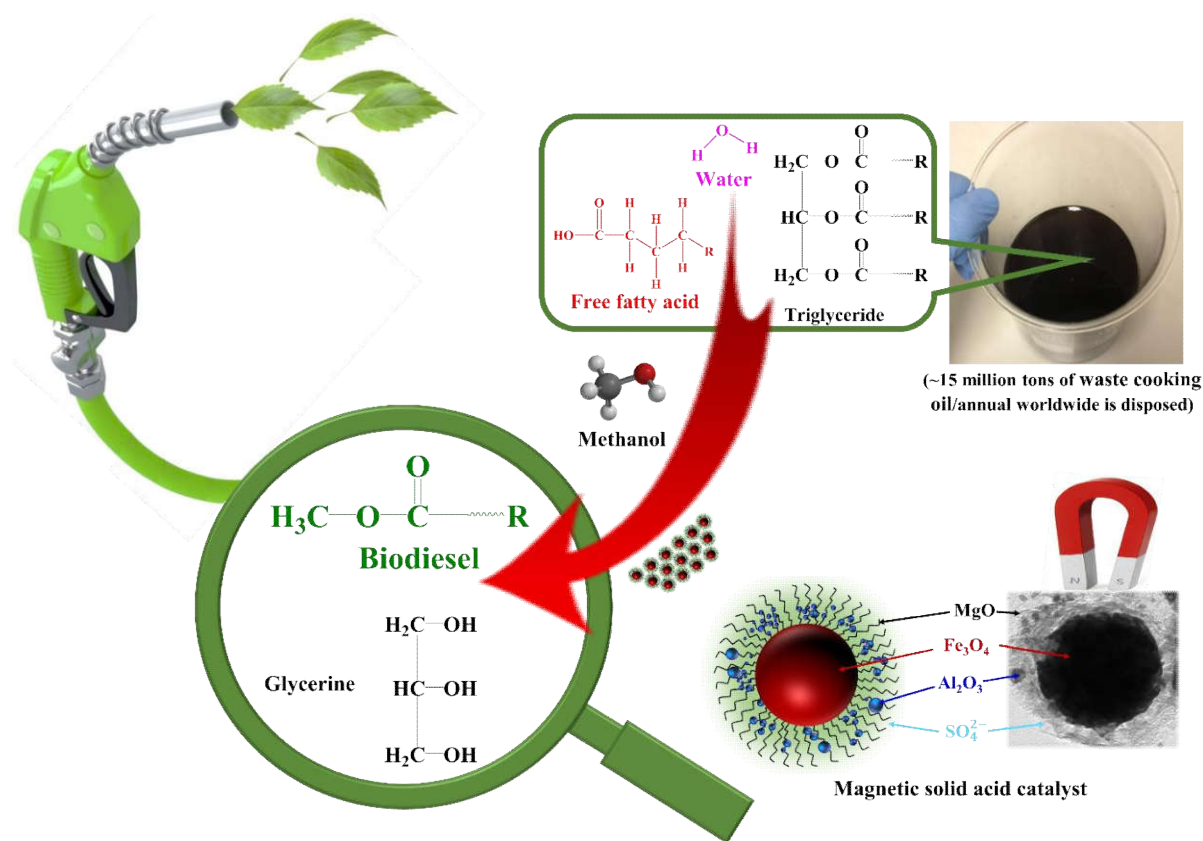


28 **Graphical abstract**

29



30

31

32 **Research highlights**

33

1. A novel magnetic solid acid catalyst was synthesised and characterised.

34

2. The catalyst was active for the (trans)esterification of WCO and oleic acid esterification.

35

3. Efficient biodiesel production from WCO is demonstrated at a low methanol:oil ratio and mild temperature.

36

37

4. Excellent catalytic stability was observed over multiple recycles.

38 **1. Introduction**

39 Energy is a key driving force for transportation, technological advancement, and industrialisation and
40 underpins global socioeconomic development [1-3]. Biodiesel, comprising fatty acid methyl esters
41 (FAME), is widely recognised as a potential low carbon alternative to fossil fuel derived diesel [4],
42 owing to its low toxicity, eco-friendliness [5, 6] and sourcing from non-edible plant and algal oils and
43 animal fats [7-9]. Oils from (micro)algae, jatropha seeds, and waste cooking oil (WCO) feedstocks have
44 been used to reduce biodiesel production costs [9-14]. For example, the amount of WCO generated in
45 the United Kingdom is estimated at 65,000 to 80,000 tons per annum while in China this figure reaches
46 1,000,000 to 2,500,000 per annum from commercial and food processing industries [15]. Such sources
47 could provide an economic alternative to virgin plant oils for biodiesel production, and valorise an
48 otherwise problematic waste stream [2]. However, untreated WCO contains high amounts of free fatty
49 acids (FFAs) and water which renders it an unsuitable feedstock for homogenous base catalysed
50 transesterification with alkaline hydroxides and methoxides due to catalyst neutralisation, hydrolysis of
51 the FAME product, and saponification and attendant separation issues due to the formation of stable
52 emulsions. Homogeneous (acid or base) catalysts also generate large quantities of contaminated
53 wastewater during biodiesel neutralisation [13, 16-19], and essential processing step to avoid engine
54 corrosion.

55 Solid acids and bases can offer good catalytic activity under mild conditions for the (trans)esterification
56 processes of WCO feedstocks [18], and enable efficient product separation and catalyst recycling, in
57 addition to continuous biodiesel production [20]. Although base catalysts are generally more active for
58 triacylglyceride (TAG) transesterification, their sensitivity to FFA contaminants (and necessity for
59 feedstock pre-treatment to remove such impurities) remain problematic [21]. Solid acid catalysts are
60 more resistant to high FFA concentrations, and can simultaneously transesterify TAGs and esterify
61 FFAs to biodiesel [22, 23]. The catalytic activity of solid acids is strongly dependent on the accessibility
62 of bulky reactants to active sites, and the number, strength, and type (Brønsted and/or Lewis) of active
63 site. Numerous solid acids have been explored for biodiesel production, including zeolites, metal oxides
64 and mixed metal oxides, supported acids, polyoxometallates, sulfonated carbons, cation exchange resins
65 and sulfated metal oxides [13, 18, 21, 24-26]. Sulfated metal oxides have attracted significant interest in
66 catalysis [23, 27-32], and are typically synthesised by the preparation of metal oxide sol gel (step 1), the
67 subsequent introduction of sulfate ions by exposure of the sol gel to sulfuric acid [H₂SO₄],

68 chlorosulfonic acid [HSO₃Cl], or ammonium sulfate [(NH₄)₂SO₄] (step 2), and a final calcination at high
69 temperature (step 3). The resulting solid superacidic features SO₄²⁻ groups at the surface on non-porous
70 metal oxide nanoparticles. The acidity of sulfated metal oxides depend on the degree of hydration,
71 preparation method and calcination temperature of the sulfated metal oxide, and the sulfate
72 concentration and presence of neighbouring strong Lewis acid sites [33, 34]. Low sulfate loadings
73 promote bidentate adsorption geometries, whereas high loadings favour Brønsted acidic polynuclear
74 (pyro)sulfates [35, 36]. Sulfated metal oxides, binary metal oxides, and ternary metal oxides are all
75 reported as promising solid acid catalysts for biodiesel production from low cost feedstocks in the
76 presence of FFAs, water, and other impurities. Studies from several authors [37-43] showed that the
77 catalytic activity of sulphated metal oxides could be improved by their fast separation from the product
78 and by-products. The magnetic catalyst has the potential to overcome the limitation for separating solid
79 acid catalysts from the reaction medium. Furthermore, the acidity of magnetic solid acid catalyst
80 reported to be stronger (H₀<-13.8) than 100% sulfuric acid (H₀=-12). For example, the uniform and
81 monodispersed iron oxide nanoparticles were designed by co-precipitation method followed by growing
82 zirconia on the surface of iron oxide nanoparticles whilst the introduction of boron oxide into the
83 solution was to inhibit the nucleation and grain growth of zirconia by delaying the phase transformation
84 of zirconia from tetragonal to monoclinic. The catalytic activity was tested at different calcination
85 temperatures (400-900 °C) for esterifying acetic acid with n-butanol. A yield of 97±1% was reported
86 under optimum conditions of 4 h, 100 °C, 850 RPM, and 1 atm nitrogen pressure [39]. Another recent
87 study by Wu and co-workers [38] reports the design of a super paramagnetic polysulphated ternary metal
88 oxides catalyst for the transesterification of cottonseeds with methyl acetate. The core was made from
89 iron oxide and prepared by co-precipitation method. Titania and zirconia was introduced to the iron
90 oxide core by another co-precipitation with different mole ratios of Zr/Ti/Fe, followed by impregnation
91 of sulphate ions from (NH₄)₂S₂O₈. The final gel was calcined at 550, 650 and 750 °C for 3 h. The
92 synthesised magnetic catalysts showed super acidity (155.3±0.9 – 598.6±1.3 μmol/g) with polysulphate
93 ions coordinated to ZrO₂-TiO₂-Fe₃O₄ catalyst support. It was reported that SO₄/ZrO₂-TiO₂-Fe₃O₄
94 catalyst calcined at 550 °C enabling a FAME yield of 99% after 10.8 h at 50 °C with 21.3 wt% of
95 catalyst and 13.8 ml of methyl acetate per g of seed. The acidity of the catalyst increased with the
96 addition of an appreciable amount of titania (3:1 mole ratio of Zr:Ti) into the catalyst texture due to the
97 formation of Zr-O-Ti units during the calcination. This resulted in more sulphur species being adsorbed
98 on the surface and inhibit the zirconia grain growth. As a result, the number of Lewis acid sites

99 increased which enhanced the catalytic activity of the catalyst. The catalyst was re-used for 8 cycles
100 with a slight decrease in activity. Alhassan et al. [37] have also designed a bifunctional magnetic
101 sulphated ternary metal oxide [Fe₂O₃-MnO-SO₄/ZrO₂] catalyst via impregnation method followed by
102 calcination at 600 °C for 3 h. This magnetic catalyst was tested for transesterification of WCO under
103 optimum conditions of 180 °C reaction temperature, 20:1 mole ratio of methanol to oil, 3 wt% of
104 catalyst loading, and 600 RPM stirring rate, where 97 ± 0.5 % of FAME yield was obtained. The loss of
105 catalytic activity reported after 6 re-runs of the spent catalyst because of pore blockage and sulphur
106 leaching. In summary, the catalytic activity of sulphated metal oxide depends mainly on the precursors,
107 type of sulfonating agent, calcination temperature, amount of sulphate content, and crystallinity of the
108 catalyst. However, there are still prone to deactivation, active site leaching, mass transport limitations,
109 low activity at lower temperatures, water sensitivity, low surface area, and difficult and/or time-
110 consuming separation by filtration or centrifugation [10, 38, 44-49]. These drawbacks highlight the
111 continuing need to design improved catalysts for esterification and transesterification of WCO. Here we
112 report the preparation of a magnetic core-shell SO₄/Mg-Al-Fe₃O₄ nanoparticle catalyst for the
113 simultaneous esterification and transesterification of WCO with methanol under mild conditions. The
114 Fe₃O₄ core facilitates magnetic separation of the solid acid catalyst from the reaction media, while the
115 encapsulating MgAlO_x shell protects the magnetic core and increases the nanoparticle surface area prior
116 to sulfation conferring good activity and stability for biodiesel production even in the presence of high
117 FFA concentrations.

118 **2. Experimental**

119 **2.1 Synthesis of magnetic core-shell SO₄/Mg-Al-Fe₃O₄ catalyst**

120 Iron oxide nanoparticles were synthesised by co-precipitation ($\text{Fe}^{2+} + 2 \text{Fe}^{3+} + 8 \text{OH}^- \rightarrow \text{Fe}_3\text{O}_4 + 4 \text{H}_2\text{O}$).
121 0.2 mol FeCl₂.4H₂O, (≥99.99 %, Sigma-Aldrich) and 0.68 mol FeCl₃.6H₂O (≥98 %, Sigma-Aldrich)
122 were separately dissolved in 25 ml of an aqueous 1:1 vol% ethanol (≥99.8 %, Sigma-Aldrich) solution
123 using an ultrasonic probe. The resulting clear solutions were added to a 250 ml round-bottomed flask,
124 and the solution pH held at 12 by dropwise addition of NH₄OH (28-30 vol%, Sigma-Aldrich), prior to
125 heating at 80 °C during stirring (250 rpm) for 6 h under a N₂ atmosphere. Following 24 ageing at room
126 temperature, iron oxide nanoparticles were isolated using an external magnetic field (Nd magnet), and
127 repeatedly rinsed with 1:1 vol% aqueous ethanol until chloride ions could not be detected in the

128 washings. The resulting dark-reddish particles were dried in an oven at 120 °C overnight, and then
129 calcined at 550 °C for 3 h to obtain Fe₃O₄ nanoparticles.

130 Magnesium oxide and alumina encapsulated Fe₃O₄ nanoparticles were synthesised as follows: 3 g of as-
131 prepared Fe₃O₄ nanoparticles were dispersed in 50 ml of 1:1 vol% aqueous isopropanol (+99.5 %,
132 Sigma-Aldrich) using an ultrasonic probe. Subsequently, 50 ml of 1:1 vol% aqueous IPA, 0.6 mol Al(O-
133 i-Pr)₃ (+98 % granular, Alfa Aesar) and 0.25 mol Mg(NO₃)₂.6H₂O (≥99.9 %, Sigma-Aldrich) were
134 added dropwise to the mixture along with 1.5 ml of HNO₃ (≥90.0 %, Sigma-Aldrich). The resulting
135 solution was mixed at room temperature for 30 min, and the pH then adjusted to 7 using NH₄OH. This
136 slurry was held at 65 °C during stirring at 250 rpm for 4 h, and then aged at room temperature overnight,
137 and the encapsulated MgO@Al₂O₃@Fe₃O₄ particles magnetically separated, washed with deionised
138 water until pH neutral, and then dried in an oven at 80 °C for 6 h before a final calcined at 550 °C for 2
139 h. The preceding nanoparticles were functionalised by sulfation. 1.0 g of as-prepared
140 MgO@Al₂O₃@Fe₃O₄ nanoparticles was added to 10 ml of 0.5 M (NH₄)₂SO₄ (≥99.5 %, VWR
141 International Ltd) aqueous solution and stirred for 6 h at room temperature. The sulfated nanoparticles
142 were magnetically separated, dried in an oven at 80 °C for 6 h, and finally calcined at 500 °C for 3 h in
143 static air. This sample is denoted SO₄/Mg-Al-Fe₃O₄.

144

145 **2.2 Catalyst characterisation**

146 Powder XRD patterns were measured using a Bruker D8 diffractometer with Cu K_α (λ=1.5418 Å)
147 radiation and a LynxEye detector between 10-70° with steps of 0.035° at 5 s per step. Particle
148 morphology, and elemental composition and spatial distributions were determined using a Hitachi
149 SU8230 cold field emission scanning electron microscope (SEM) operated at 2 kV, and FEI Titan
150 Themis Cubed 300 transmission electron microscope (TEM) coupled with an Oxford INCA energy
151 dispersive X-ray spectrometer (EDS). For the TEM analysis magnetic nanoparticles were dispersed in
152 acetone and then drop cast on a carbon coated copper grid. Surface functional groups were examined at
153 room temperature using a Nicolet iS10 FTIR spectrometer by attenuated total reflectance (ATR) between
154 550-4000 cm⁻¹ at a resolution of 4 cm⁻¹. Textural properties were obtained by N₂ physisorption method at
155 77 K using a Micromeritics TriStar 3000 porosimeter. The as-prepared magnetic catalyst was degassed
156 in vacuo at 120 °C for 16 h prior to analysis, and the surface area calculated using the Brunauer–
157 Emmett–Teller (BET) method over the relative pressure (p/p₀) range 0.05-0.2, with pore size distributions

158 determined by the Barrett-Joyner-Halenda (BJH) method applied to the desorption isotherm.
159 Thermogravimetric analysis (TGA) was performed using a Mettler Toledo TGA/DSC-2 instrument
160 under N₂ gas at 50 ml min⁻¹ and a heating rate of 10 °C min⁻¹ from 25 to 900 °C. Total sulfate loadings
161 were determined from the mass loss by TGA between 600-900 °C and using a Thermo Scientific™
162 FLASH 2000 CHNS-O elemental analyser. Metal loadings were determined using a PerkinElmer Sciex
163 inductively coupled plasma-mass spectroscopy (ICP-MS). Acid site loadings were quantified by n-
164 propylamine chemisorption and subsequent temperature programmed desorption (TPD) under flowing He
165 at 30 ml min⁻¹ and a heating rate of 10 °C min⁻¹ from 40 to 800 °C. The catalyst was first saturated with
166 n-propylamine, and physisorbed species removed by in vacuo drying at 30 °C overnight [5]. Thermal
167 desorption of reactively-formed propene (m/z=41) and ammonia (m/z=17) from propylamine
168 decomposition was monitored using a Pfeiffer ThermoStar quadupole mass spectrometer.

169 **2.3 Catalyst testing**

170 **2.3.1 Esterification and transesterification of WCO**

171 WCO was obtained from a restaurant in Leeds, and contained 0.14 wt% moisture and 2 wt% FFA [5].
172 Transesterification and esterification was conducted in a stirred glass batch reactor connected to a
173 Ministat Huber 125 Pilot ONE Controller temperature controller and reflux condenser. The WCO was
174 pre-treated by simple filtration to remove physical impurities, and then heated to 100 °C to remove
175 water. Physicochemical properties of the waste cooking oil were measured after this pre-treatment. Pre-
176 treated WCO was mixed with methanol (≥99.9 %, HPLC grade Sigma-Aldrich) to achieve the desired
177 molar ratio and added to the glass reactor at room temperature, together with the desired mass of
178 SO₄/Mg-Al-Fe₃O₄ catalyst. The reaction mixture was then stirred at 600 rpm and heated to the required
179 temperature. Aliquots of the mixture were periodically sampled for off-line GC-MS analysis using a
180 Perkin Elmer Clarus 580S gas chromatograph, equipped with an Elite 5ms capillary column (30.0 m x
181 250 μm) and a 560S mass spectrometer [45].

182 **2.3.2 Esterification of oleic acid**

183 The stability of SO₄/Mg-Al-Fe₃O₄ catalyst was assessed during oleic acid esterification as a model FFA
184 using the optimised process parameters for biodiesel production from WCO. 4.0 wt% of SO₄/Mg-Al-
185 Fe₃O₄ catalyst and 9:1 molar ratio of methanol: oleic acid (Fluka Analytical, ≥99) were charged into
186 the glass reactor at room temperature. The three-phase mixture (solid-liquid-liquid) was agitated at 600

187 RPM and heated to 95 °C. Methyl oleate formation was periodically monitored by withdrawing sample
188 aliquots and off-line GC-MS analysis [45].

189 **2.4 Biodiesel characterisation**

190 A Setaflash series 3 closed cup automated flash point tester was used to capture the flash point of the
191 synthetic biodiesel under a temperature ramp of 1-2 °C min⁻¹. The biodiesel density was calculated using
192 a pycnometric method at 15 °C, and kinematic viscosity measured at 40 °C by a Malvern Bohlin-Gemini
193 150 rotary rheometer. Acid values and %FFA of the synthetic biodiesel were measured according to
194 standard methods [5]. Free glycerol, mono-, di-, triglyceride and total glycerine contents were quantified
195 using a Perkin Elmer Clarus 560 GC equipped with an on-column injection system, a flame ionization
196 detector and a capillary column (15.0 m x 0.32 mm, 0.1 µm) [50, 51]. The total FAME (biodiesel) yield
197 was determined by off-line GC-MS using a modified EN-14103 procedure as previously reported [45]
198 from **Equation 1**:

$$200 \quad \text{Total FAME \%} = \frac{(\sum A) - A_{IS}}{A_{IS}} * \frac{C_{IS} * V_{IS}}{W} * 100 \quad \text{Eqn. (1)}$$

201

202 where $\sum A$ =total peak area of methyl esters, A_{IS} =peak area of methyl heptadecanoate, C_{IS} =methyl
203 heptadecanoate concentration in mg/ml, V_{IS} =used volume of methyl heptadecanoate solution in ml, and
204 W =sample mass in mg.

205

206 **2.5 Catalyst reusability and leaching**

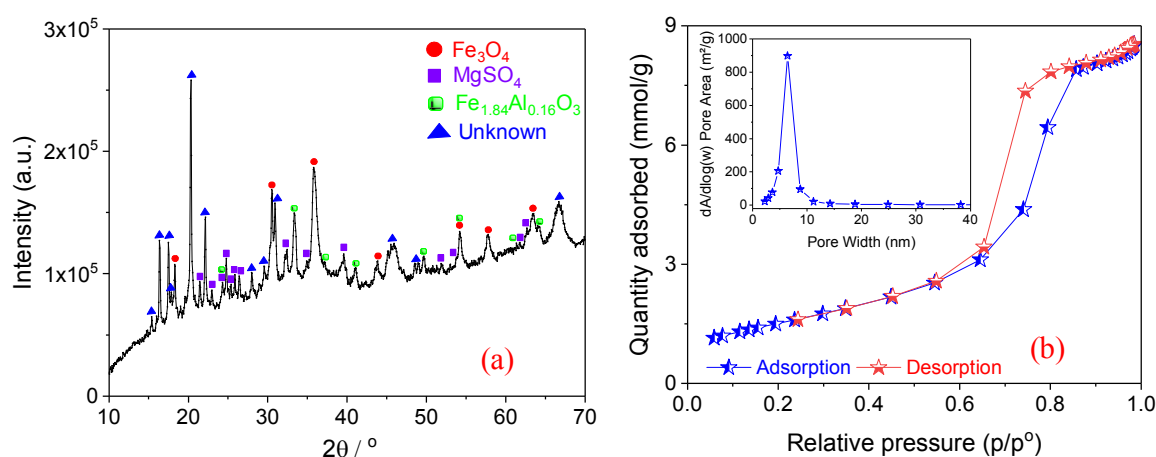
207 Catalyst reusability for biodiesel production from WCO was assessed by magnetically separating the
208 post-reaction catalyst from the reaction mixture, washing the catalyst repeatedly with a 1:1 vol%
209 methanol:n-hexane mixture to remove any weakly bound organic residues, and then a final 250 °C re-
210 calcination for 2 h to remove any chemisorbed organics, moisture or CO₂ on the catalyst surface.
211 Leaching from the SO₄/Mg-Al-Fe₃O₄ catalyst was investigated by ICP-MS. A sample of the synthetic
212 biodiesel was digested after each reaction using a HF100-multiwave 3000 (Anton Paar) microwave
213 digester using 7.0 ml of concentrated nitric acid (≥69%, Fluka Analytical, TraceSELECT[®]), 1.0 ml of
214 concentrated fuming hydrochloric acid (≥37%, Fluka Analytical, TraceSELECT[®]) and 2.0 ml of
215 hydrogen peroxide (~30%, Sigma-Aldrich, for ultra-trace analysis) reagents. The resulting solutions

216 were diluted with deionised water to 50 ml and then nebulised into the ICP. Mg, S, Al, and Fe
217 concentrations were determined by standard methods [50].

218 3. Results and discussion

219 3.1 Catalyst characterisation

220 Powder XRD of the as-prepared SO₄/Mg-Al-Fe₃O₄ (**Figure 1a**) revealed sharp reflections at 18.3, 30.2,
221 35.5, 37.2, 43.2, 53.6, 57.1, and 62.7°, assigned to the [111], [220], [311], [222], [400], [422], [511] and
222 [440] planes of cubic Fe₃O₄ (magnetite, ICDD: 04-002-3668) respectively. Particle size analysis
223 applying the Scherrer equation to peak widths indicates volume-averaged Fe₃O₄ crystalline diameters of
224 86 nm. Reflections were also observed at 24.3, 33.4, 35.8, 41.1, 49.7, 54.4, 62.8, and 64.4° assigned to
225 the [012], [104], [110], [113], [024], [116], [214] and [300] planes respectively of rhombohedral
226 Fe_{1.84}Al_{0.16}O₃ (iron aluminium oxide, ICDD: 04-005-8669). Weak reflections are also present between
227 2θ=20-65°, attributed to orthorhombic magnesium sulfate (MgSO₄, ICDD: 00-021-0546) with cell
228 parameters a=4.75, b=8.59 and c=6.71 Å.
229



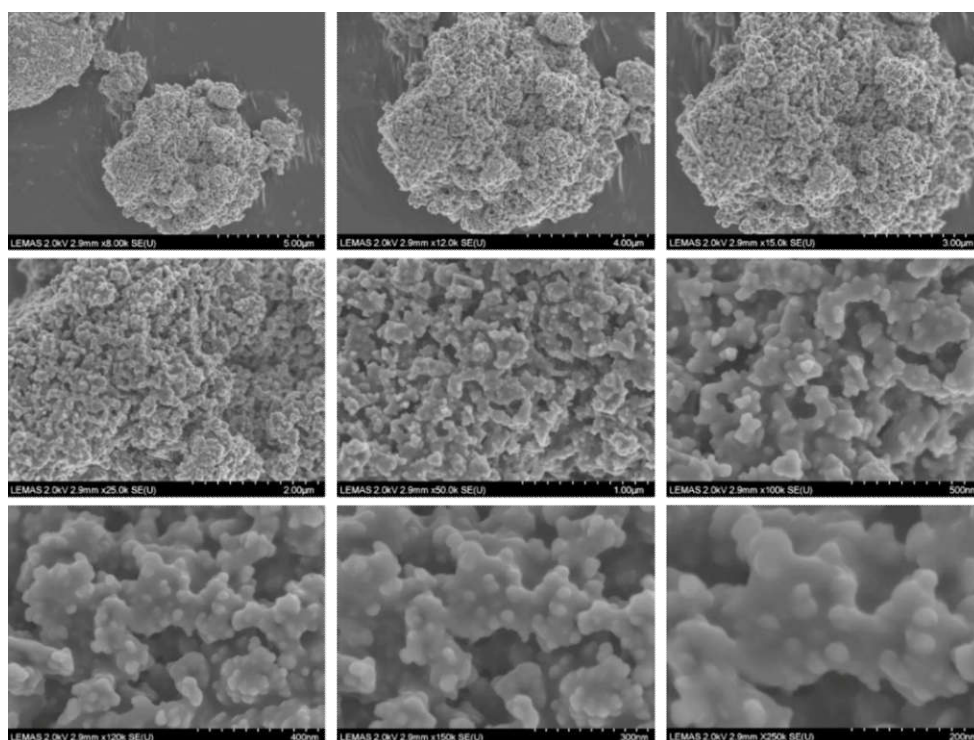
230

231 **Figure 1.** (a) Powder XRD pattern, and (b) N₂ adsorption-desorption isotherms and mean pore sizes
232 (inset) of as-prepared SO₄/Mg-Al-Fe₃O₄.

233
234

235 Porosimetry of SO₄/Mg-Al-Fe₃O₄ showed a Type IV isotherm (**Figure 1b**) and type H1 hysteresis loop
236 [52] which are typically associated with capillary condensation within cylindrical mesopores. Since the
237 synthesis did not employ a structure-directing template, these mesopores may arise from interparticle
238 voids, but in any even could serve to improve reactant accessibility to active sites. SEM images of the

239 $\text{SO}_4/\text{Mg-Al-Fe}_3\text{O}_4$ catalyst reveal the formation of large (~20-40 nm) nanoparticle aggregates (**Figure 2**)
240 which are embedded in a (presumably amorphous alumina and/or MgSO_4) matrix to form a coral-like
241 porous architecture. TEM images confirm the presence of (high contrast) Fe_3O_4 cores between 20-150
242 nm diameter, encapsulated by amorphous shells comprising low contrast aggregates of (presumably
243 Al/Mg-rich) of ~5-15 nm nanoparticles (**Figure 3**). Elemental maps confirm that Fe_3O_4 nanoparticles are
244 embedded within an Al-rich matrix (**Figure 4**), with Mg co-located with S in a 1:1 atomic ratio. The
245 atomic ratio of Al:Mg = 6:1 throughout the sample which may suppress nucleation and growth of Mg-Al
246 hydroxalicates (unstable for values >4:1), whereas that for Fe:Mg = 3:1 [53]. The low magnesium content
247 of the as-prepared catalyst may also reflect the low pH used during its synthesis. The total sulfur content
248 determined by TEM-EDS, CHNS-O, and ICP-MS was approximately 7 wt% (**Table 1**), higher than that
249 reported for SO_4/MO_x (2-3 wt%) [54] and Al-doped SO_4/ZrO_2 (1.5 wt%) [55], but comparable to
250 $\text{SO}_4/\text{Fe-Al-TiO}_2$ [5].



251

252

253

254

Figure 2. SEM images at different magnifications for $\text{SO}_4/\text{Mg-Al-Fe}_3\text{O}_4$ catalyst.

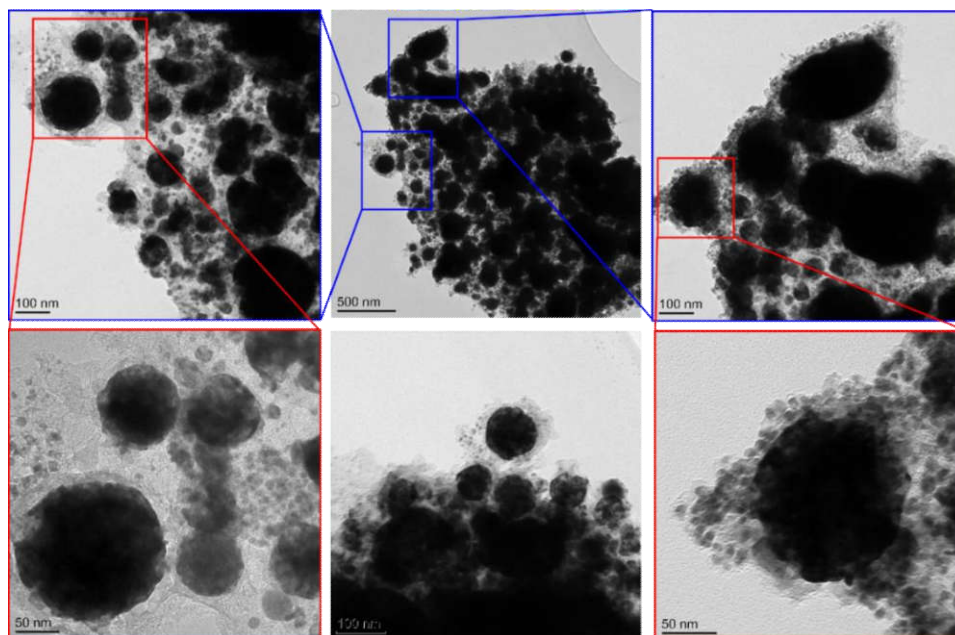


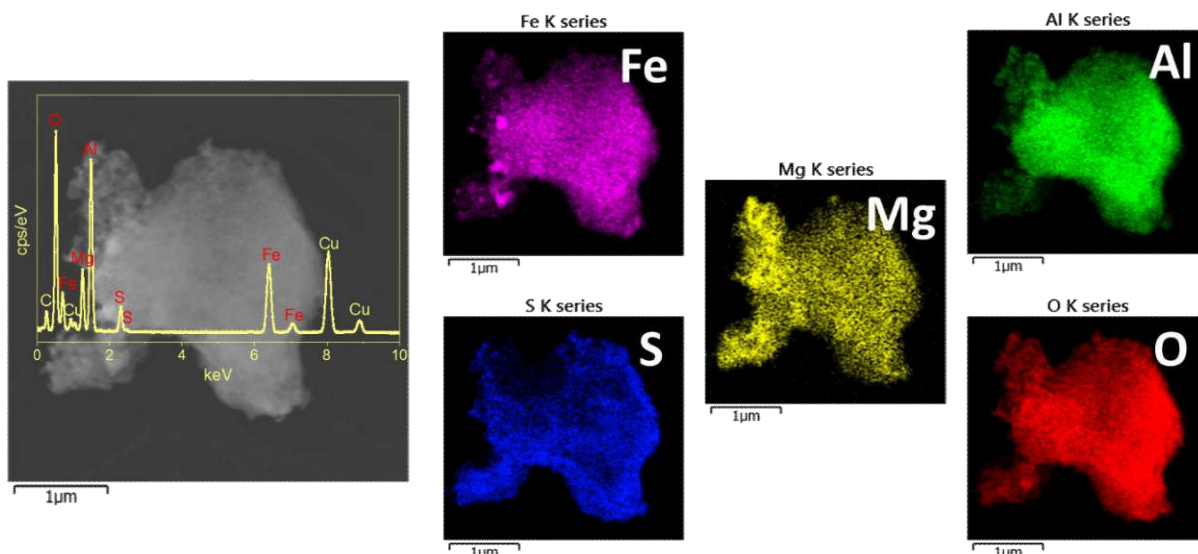
Figure 3. TEM images of SO₄/Mg-Al-Fe₃O₄ catalyst.

Table 1. Textural properties and composition of SO₄/Mg-Al-Fe₃O₄.

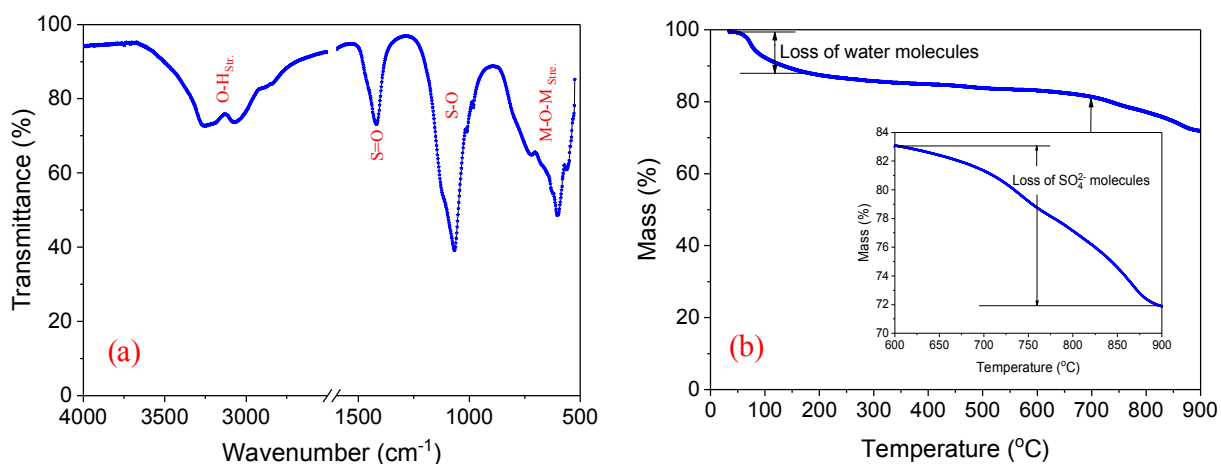
	Textural properties ^a			Composition / atom% ^b					Bulk S content/ wt%	
	S _{BET} / m ² g ⁻¹	D _p / nm	V _p / cm ³ g ⁻¹	O	Mg	Al	S	Fe		
SO ₄ /Mg-Al-Fe ₃ O ₄	123 ± 1	6.5 ± 0.5	0.3	60.5	3.5	20.7	4.6	10.7	7.8 ± 1 ^c	7.6 ± 0.5 ^d

^aN₂ porosimetry. ^bEDS. ^cCHNS-O. ^dICP-MS.

The ATR-IR spectrum of SO₄/Mg-Al-Fe₃O₄ exhibited a strong broad band at 3252 cm⁻¹ attributed to the O-H stretch of physisorbed water (**Figure 5a**) on the surface of the catalyst from the air and/or interlayer water molecules while the peak at 3072 cm⁻¹ corresponded to the O-H stretching vibration of bound water [5, 38, 56]. The strong bands between 982-1087 cm⁻¹ are assigned to chelating bidentate sulfate (SO₄²⁻) and/or chelating double-bridge peroxydisulfate (S₂O₈²⁻) groups, and that at 1418 cm⁻¹ to an S=O stretch [38, 39]. Bands at 719, 604, and 566 cm⁻¹ likely arise from to M-O-M stretches involving Al-O, Mg-O and Fe-O bonds [38, 56-59].



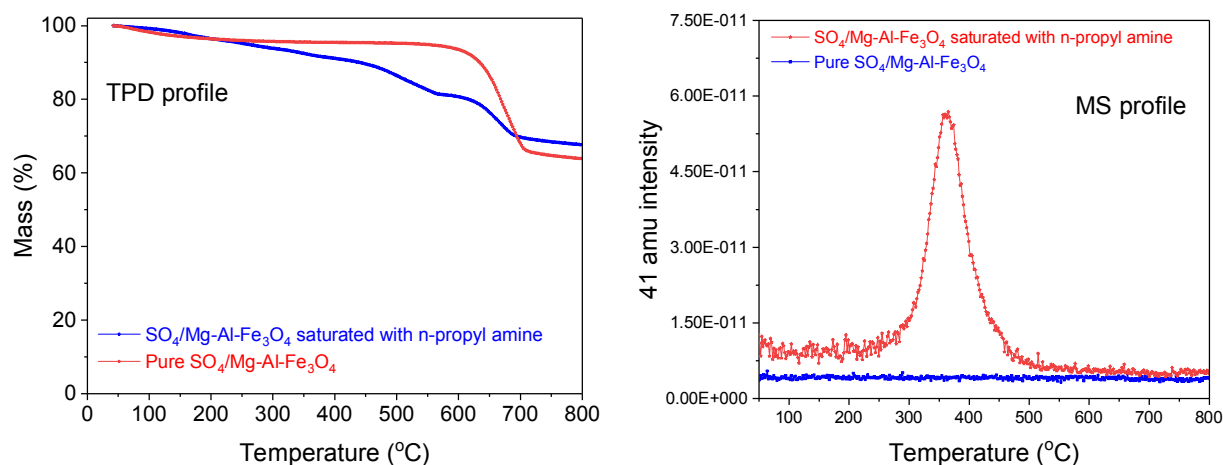
269
270
271
272
Figure 4. EDS elemental mapping of $\text{SO}_4/\text{Mg-Al-Fe}_3\text{O}_4$ catalyst.



273
274
275
Figure 5. (a) FTIR spectrum and (b) TGA profile of $\text{SO}_4/\text{Mg-Al-Fe}_3\text{O}_4$.

276 TGA of the as-prepared $\text{SO}_4/\text{Mg-Al-Fe}_3\text{O}_4$ exhibited two distinct weight losses (**Figure 5b**). The first,
277 between 100 and 150 °C, is associated with the loss of physisorbed water [60], and the second between
278 600-900 °C is due to the decomposition of sulfate and/or peroxydisulfate groups and SO_x evolution [5];
279 sulfate species are thermally stable <600 °C, superior to that observed for other sulfated metal oxides
280 [39, 61]. The sulfate loading calculated from TGA of 11 wt% is in good agreement with elemental
281 analysis. Acid loading and strength of the as-prepared catalyst were quantified by n-propylamine TPD-
282 MS (**Figure 6**). A strong desorption peak for reactively-formed propene is observed between 300-500

283 °C (arising from Hofmann elimination of chemisorbed n-propylamine over acid sites) indicative of
284 moderate strength acid sites akin to those reported in SO_4/ZrO_2 [32]. The calculated total acidic site
285 loadings of the $\text{SO}_4/\text{Mg-Al-Fe}_3\text{O}_4$ catalyst were found to be 2.35 mmol g^{-1} which is much higher than
286 that reported for other sulfated metal oxides (typically $<1 \text{ mmol g}^{-1}$) [5, 62, 63].
287

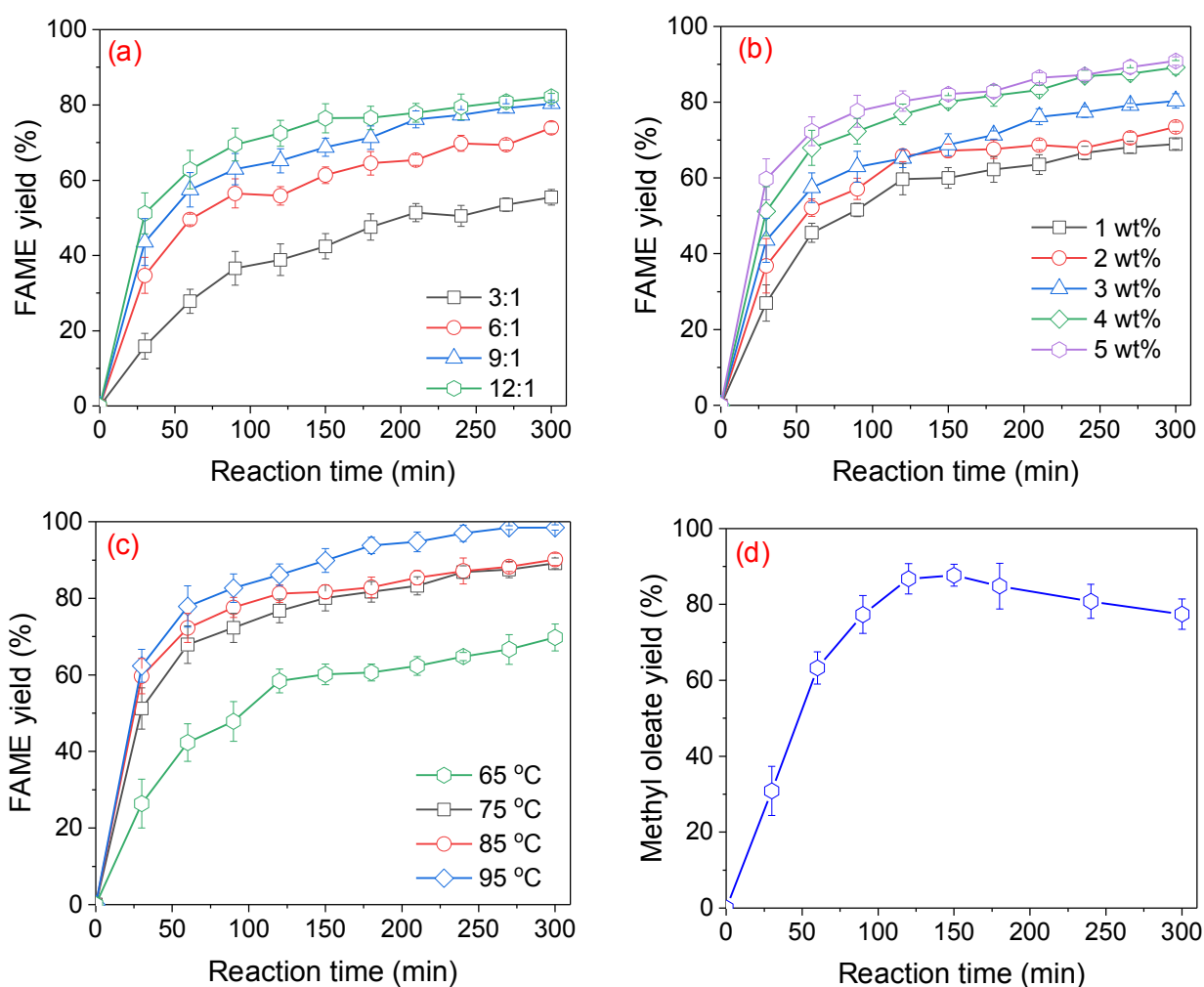


288
289 **Figure 6.** (left) TPD profiles, and (right) mass spectra for $\text{SO}_4/\text{Mg-Al-Fe}_3\text{O}_4$ catalyst of pure and
290 saturated with n-propylamine.
291

292 3.2 Catalytic performance

293 The as-prepared $\text{SO}_4/\text{Mg-Al-Fe}_3\text{O}_4$ catalyst was subsequently evaluated for biodiesel production from
294 WCO (**Figure 7**). First, the effect of methanol:WCO molar ratio was explored between 3:1 to 12:1;
295 increasing the methanol content monotonically enhanced the 6 h FAME yield from approximately 55 to
296 80 % by shifting the transesterification reaction equilibrium (**Figure 7a**). Since only a small yield
297 enhancement was observed for methanol:WCO ratios $>9:1$, this reaction composition was employed for
298 all further experiments. Increasing the catalyst mass (with respect to WCO) from 1 to 5 wt% linearly
299 improved the initial FAME yield (**Figure 7b**), indicating that transesterification was free from mass-
300 transport limitations during the first hour of reaction reflecting the rise in active sites preceding a slow
301 deactivation at longer reaction times [64]. Final 6 h FAME yields spanned 65-80 %. A catalyst loading
302 of 3 wt% was selected as this provided a sufficient yield to measure accurately, while offering scope for
303 improvements during further optimisation without encountering diffusion limitations. The impact of
304 reaction temperatures was also studied between 65 to 95 °C (**Figure 7c**) [45]. A significant yield
305 increase was observed on raising the reaction temperature to 75 °C (followed by a more gradual rise at

306 higher temperature) which may both reflect both enhanced rates of TAG hydrolysis and better
 307 miscibility of the methanol/WCO liquid phases, as previously reported [65, 66]. The maximum 6 h
 308 FAME yield >95 % at the highest temperature. To establish the catalyst tolerance to FFAs, oleic acid
 309 esterification with methanol was also examined under the optimum reaction conditions (**Figure 7d**).
 310 SO₄/Mg-Al-Fe₃O₄ catalyst was active for methyl oleate production, with a maximum FAME yield of 87
 311 % after 2 h reaction; the small drop in FAME yield at longer reaction times may be associated with
 312 water (by-product) accumulation driving the reverse hydrolysis.



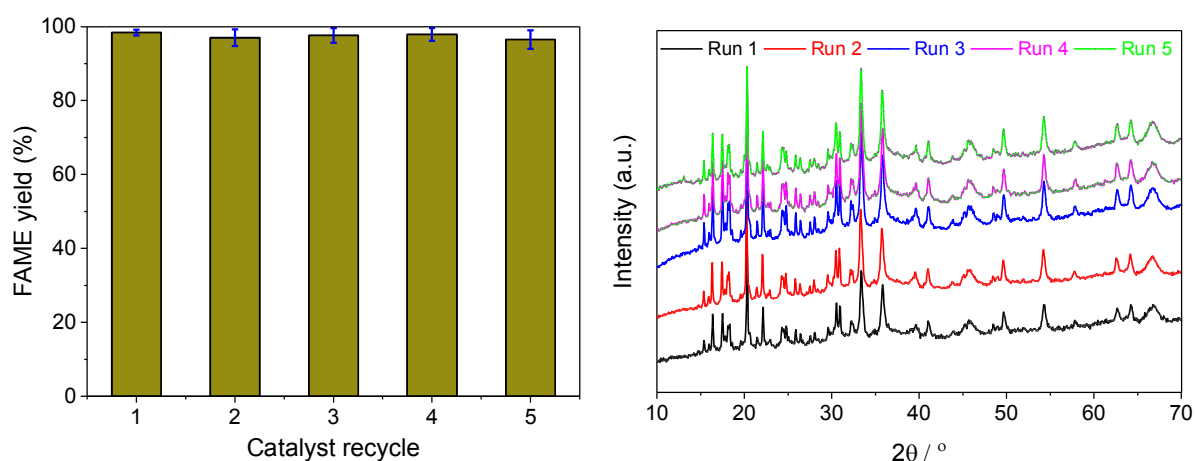
314
 315 **Figure 7.** WCO transesterification over SO₄/Mg-Al-Fe₃O₄ as a function of (a) methanol:WCO molar
 316 ratio at 75 °C and 3 wt% catalyst, (b) catalyst loading at 75 °C and 9:1 methanol:WCO molar ratio, and
 317 (c) reaction temperature at 4 wt% catalyst and 9:1 methanol:WCO molar ratio. (d) Oleic acid
 318 esterification over SO₄/Mg-Al-Fe₃O₄ at 95 °C, 4 wt% catalyst, and 9:1 methanol:oleic acid molar ratio.

319

320 **3.3 Magnetic catalyst reusability and leaching**

321 Stability of $\text{SO}_4/\text{Mg-Al-Fe}_3\text{O}_4$ for WCO transesterification was investigated during five catalyst re-uses
 322 under optimal reaction conditions (**Figure 8**). Minimal deactivation was observed, consistent with post-
 323 reaction XRD analysis of the catalyst which evidenced negligible change in the phase or crystallinity,
 324 and elemental analysis which revealed negligible metal or sulfur leaching occurred into the reaction
 325 medium (**Table 2**). A small increase in the residual Al and Fe concentrations in the biodiesel product
 326 was observed for Run 3, attributed to the use of a different strength magnet to separate the nanoparticles
 327 compared with the other four runs. This excellent stability is an important consideration for commercial
 328 (large scale) biodiesel production from low grade oil feedstocks.

329



330

331 **Figure 8. (left)** Transesterification of WCO over $\text{SO}_4/\text{Mg-Al-Fe}_3\text{O}_4$ as a function of re-use: reaction
 332 conditions: 4 wt%, 95 °C, 9:1 methanol:WCO molar ratio. **(right)** XRD patterns of post-reaction
 333 $\text{SO}_4/\text{Mg-Al-Fe}_3\text{O}_4$.

334

335

336

Table 2. Elemental analysis of biodiesel after magnetic catalyst separation.

		Leachate concentration ^a / $\mu\text{g L}^{-1}$			
		Mg	Al	S	Fe
Spent catalyst	Run 1	0.343	0.124	0.000	0.082
	Run 2	0.308	0.098	0.000	0.028
	Run 3	0.356	0.378	0.000	0.229
	Run 4	0.327	0.120	0.000	0.067
	Run 5	0.220	0.082	0.000	0.053

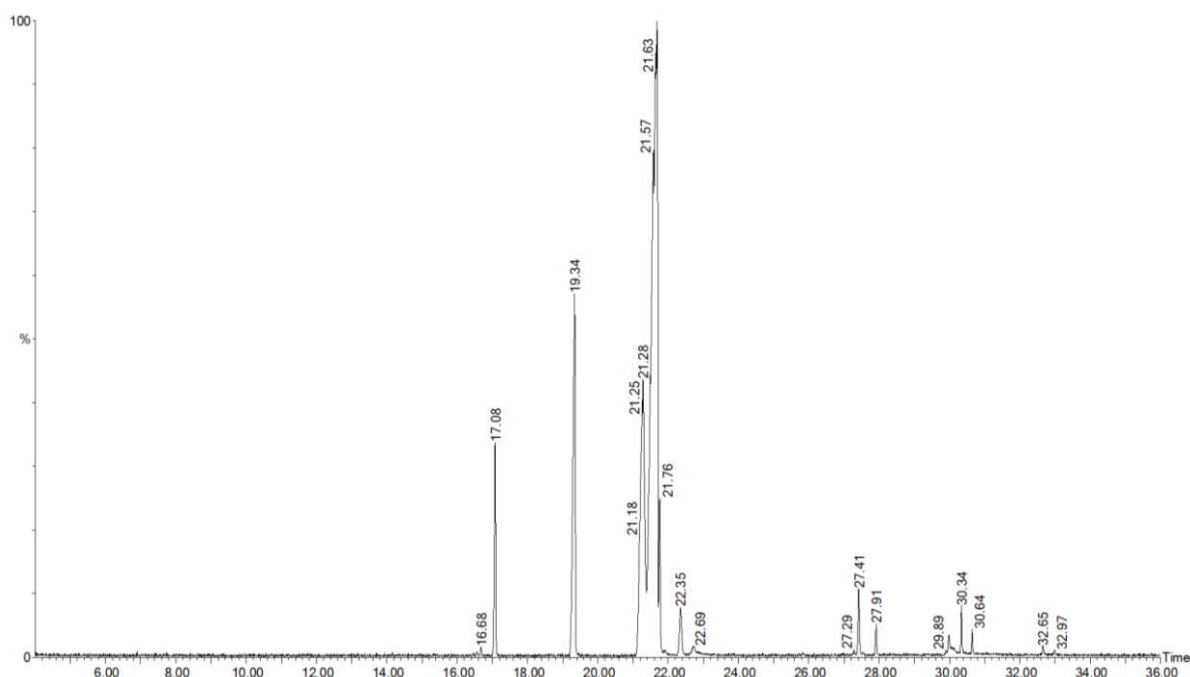
337

^a ICP-MS.

338 **3.3 Biodiesel characterisation**

339 Analysis of the transesterification biodiesel product is critical to determining the quality of any ultimate
340 fuel blend due to the potential presence of contaminants including glycerol, FFAs, catalyst residue,
341 methanol, and water. GC-MS analysis (**Figure 9**) of the biodiesel product was therefore conducted to
342 quantify the biodiesel purity, using a response factor from the methyl heptanoate internal standard
343 (≥ 99.5 purity, Sigma-Aldrich) to calculate the amount of individual FAME components (**Table 3**). The
344 major FAME products were methyl palmitate, methyl stearate, methyl oleate, methyl linoleate, methyl
345 linoleate, and methyl gadoleate. The physicochemical properties of the biodiesel confirm that its quality
346 meets ASTM and EU standards (**Table 4**).

347



348

349 **Figure 9.** GC-MS chromatogram for biodiesel product from WCO transesterification over $\text{SO}_4/\text{Mg-Al-}$
350 Fe_3O_4 . Reaction conditions: 4 wt% catalyst mass to WCO, 95 °C, 9:1 methanol:WCO molar ratio

351

352

353

354

355

356

357 **Table 3.** FAME composition of biodiesel derived from WCO transesterification over $\text{SO}_4/\text{Mg-Al-Fe}_3\text{O}_4$

FAME	Chain structure	Retention time / mins	Area	FAME / Area %
Myristic acid methyl ester	C _{14:0}	14.157	528458	0.04
Palmitic acid methyl ester	C _{16:0}	17.074	66629604	5.01
Palmitoleic acid methyl ester	C _{16:1}	16.673	2244707	0.17
Heptadecanoic acid methyl ester	C _{17:0}	19.334	195359776	IS
Stearic acid methyl ester	C _{18:0}	22.351	26016648	1.96
Oleic acid methyl ester	C _{18:1}	21.675	898642007	67.77
Linoleic acid methyl ester	C _{18:2}	21.280	279073632	20.99
Linolenic acid methyl ester	C _{18:3}	21.675	17771433	1.17
Gadoleic acid methyl ester	C _{20:1}	27.413	20598874	1.55
Erucic acid methyl ester	C _{21:1}	30.334	11479104	0.86
Behenic acid methyl ester	C _{22:0}	30.639	5037719	0.38
Lignoceric acid methyl ester	C _{24:0}	30.980	1328256	0.10

358

359

360

Table 4. Properties of biodiesel derived from WCO transesterification over $\text{SO}_4/\text{Mg-Al-Fe}_3\text{O}_4$

Property	Unit	Limits		Synthesised biodiesel
		ASTM D6751	EN14214	
Flash point	°C	93 min.	101 min.	179.5
Kinematic viscosity	mm ² s ⁻¹	1.9-6.0	3.5-5.0	4.74
Acid number	mgKOH g ⁻¹	0.8 max.	0.5 max.	0.34
Density at 15 °C	kg m ⁻³	---	860-900	892.6
FAME content	% mass	---	96.5 min.	98.5
Methyl linolenate content	% mass	---	12 max.	1.17
Free glycerine content	% mass	0.02 max.	---	0.025
Total glycerine content	% mass	0.24 max.	0.25 max.	0.122
Monoglyceride content	% mass	---	0.8 max.	0.007
Diglyceride content	% mass	---	0.2 max.	0.008
Triglyceride content	% mass	---	0.2 max.	0.082

361 **4. Conclusions**

362 A novel magnetically separable $\text{SO}_4/\text{Mg-Al-Fe}_3\text{O}_4$ core-shell catalyst was synthesised for the
 363 transesterification of WCO and esterification of oleic acid. Bulks and surface physicochemical
 364 properties were characterised by XRD, SEM, TEM, TGA, ATR-FTIR, N₂ porosimetry, and propylamine
 365 TPD-MS. Magnetic Fe₃O₄ (20-150 nm diameter) nanoparticles were encapsulated by 5-15 nm thick
 366 alumina and/or MgSO₄ shells. Sulfation generated surface bidentate sulfate ions which exhibited

367 moderate acid strengths but high acid site loadings of 2.35 mmol g⁻¹. The multifunctional catalyst
368 properties (super acidity and magnetic separability) pave the way for simultaneous esterification and
369 transesterification of low grade bio-oil feedstocks to biodiesel, eliminating the need for current pre-
370 treatments to reduce the FFA content, and enabling facile and energy efficient product separation. The
371 SO₄/Mg-Al-Fe₃O₄ catalyst exhibited good activity for biodiesel production from WCO for a 9:1
372 methanol:oil molar ratio and 4 wt% catalyst loading after 5 h reaction at 95 °C. It also exhibited good
373 activity for oleic acid esterification (87 % yield in 2 h) under similar reaction conditions, highlighting
374 the potential of SO₄/Mg-Al-Fe₃O₄ for the direct conversion of low grade oil feedstocks high in FFAs to
375 biodiesel, without requiring any pre-treatment. SO₄/Mg-Al-Fe₃O₄ demonstrates excellent stability and
376 recyclability over five consecutive transesterification reactions with negligible deactivation or leaching,
377 paving the way to commercial biodiesel production from WCO using a heterogeneous catalyst. Future
378 study could involve investigation of the effect of different calcination temperatures on the catalytic
379 performance of this magnetic catalyst. An extended study should also focus on the investigation of
380 mechanism of this catalyst for esterification and transesterification reactions. Tests of different chain
381 length of fatty acid composition feedstocks need to be carried out in order to better understand its effect
382 on the performance of this type of catalyst as WCO is a mixture of different fatty acids.

383

384 **Acknowledgments**

385 The authors are gratefully acknowledge the Ministry of Higher Education and Scientific Research of the
386 Kurdistan Regional Government for funding this study under the Human Capacity Development Program
387 (HCDP).

388

389 **Conflicts of interest**

390 The authors declare no conflict of interest.

391

392 **References**

- 393 1. Atabani, A.E., A.S. Silitonga, I.A. Badruddin, T. Mahlia, H. Masjuki, and S. Mekhilef, *A*
 394 *comprehensive review on biodiesel as an alternative energy resource and its characteristics*.
 395 *Renewable and sustainable energy reviews*, **2012**. 16(4): p. 2070-2093.
- 396 2. Wilson, K. and A.F. Lee, *Rational design of heterogeneous catalysts for biodiesel synthesis*.
 397 *Catalysis Science & Technology*, **2012**. 2(5): p. 884-897.
- 398 3. Melero, J.A., L.F. Bautista, G. Morales, J. Iglesias, and R. Sánchez-Vázquez, *Biodiesel*
 399 *production from crude palm oil using sulfonic acid-modified mesostructured catalysts*. *Chemical*
 400 *Engineering Journal*, **2010**. 161(3): p. 323-331.
- 401 4. Younis, K.A., J.L. Gardy, and K.S. Barzinji, *Production and characterization of biodiesel from*
 402 *locally sourced sesame seed oil, used cooking oil and other commercial vegetable oils in Erbil-*
 403 *Iraqi Kurdistan*. *American Journal of Applied Chemistry*, **2014**. 2(6): p. 105-111.
- 404 5. Gardy, J., A. Osatiashtiani, O. Céspedes, A. Hassanpour, X. Lai, A.F. Lee, K. Wilson, and M.
 405 Rehan, *A magnetically separable SO₄/Fe-Al-TiO₂ solid acid catalyst for biodiesel production*
 406 *from waste cooking oil*. *Applied Catalysis B: Environmental*, **2018**. 234: p. 268-278.
- 407 6. Gardy, J., A. Hassanpour, X. Lai, and M. Rehan, *The influence of blending process on the*
 408 *quality of rapeseed oil-used cooking oil biodiesels*. *International Scientific Journal (Journal of*
 409 *Environmental Science)*, **2014**. 3: p. 233-240.
- 410 7. Silva, Â., K. Wilson, A.F. Lee, V.C. dos Santos, A.C.C. Bacilla, K.M. Mantovani, and S.
 411 Nakagaki, *Nb₂O₅/SBA-15 catalyzed propanoic acid esterification*. *Applied Catalysis B:*
 412 *Environmental*, **2017**. 205: p. 498-504.
- 413 8. Creasey, J.J., A. Chieragato, J.C. Manayil, C.M. Parlett, K. Wilson, and A.F. Lee, *Alkali-and*
 414 *nitrate-free synthesis of highly active Mg–Al hydrotalcite-coated alumina for FAME production*.
 415 *Catalysis Science & Technology*, **2014**. 4(3): p. 861-870.
- 416 9. Rehan, M., J. Gardy, A. Demirbas, U. Rashid, W. Budzianowski, D. Pant, and A. Nizami, *Waste*
 417 *to biodiesel: A preliminary assessment for Saudi Arabia*. *Bioresource technology*, **2018**. 250: p.
 418 17-25.
- 419 10. Alhassan, F.H., U. Rashid, and Y.H. Taufiq-Yap, *Synthesis of waste cooking oil based biodiesel*
 420 *via ferric-manganese promoted molybdenum oxide/zirconia nanoparticle solid acid catalyst:*
 421 *influence of ferric and manganese dopants*. *Journal of oleo science*, **2015**. 64(5): p. 505-514.
- 422 11. Nisar, J., R. Razaq, M. Farooq, M. Iqbal, R.A. Khan, M. Sayed, A. Shah, and I. ur Rahman,
 423 *Enhanced biodiesel production from Jatropha oil using calcined waste animal bones as catalyst*.
 424 *Renewable Energy*, **2017**. 101: p. 111-119.
- 425 12. Li, L., C. Zou, L. Zhou, and L. Lin, *Cucurbituril-protected Cs_{2.5}H_{0.5}PW₁₂O₄₀ for optimized*
 426 *biodiesel production from waste cooking oil*. *Renewable energy*, **2017**. 107: p. 14-22.
- 427 13. Lee, A.F., *Catalysing sustainable fuel and chemical synthesis*. *Applied Petrochemical Research*,
 428 **2014**. 4(1): p. 11-31.
- 429 14. Raia, R.Z., L.S. da Silva, S.M.P. Marcucci, and P.A. Arroyo, *Biodiesel production from*
 430 *Jatropha curcas L. oil by simultaneous esterification and transesterification using sulphated*
 431 *zirconia*. *Catalysis Today*, **2017**. 289: p. 105-114.
- 432 15. Upham, P., P. Thornley, J. Tomei, and P. Boucher, *Substitutable biodiesel feedstocks for the UK:*
 433 *a review of sustainability issues with reference to the UK RTFO*. *Journal of Cleaner Production*,
 434 **2009**. 17: p. S37-S45.

- 435 16. Pirez, C., A. Lee, J.C. Manayil, C. Parlett, and K. Wilson, *Hydrothermal saline promoted*
436 *grafting: a route to sulfonic acid SBA-15 silica with ultra-high acid site loading for biodiesel*
437 *synthesis*. Green Chemistry, **2014**. 16(10): p. 4506-4509.
- 438 17. Montero, J., M. Isaacs, A. Lee, J. Lynam, and K. Wilson, *The surface chemistry of*
439 *nanocrystalline MgO catalysts for FAME production: An in situ XPS study of H₂O, CH₃OH and*
440 *CH₃OAc adsorption*. Surface Science, **2016**. 646: p. 170-178.
- 441 18. Lee, A.F. and K. Wilson, *Recent developments in heterogeneous catalysis for the sustainable*
442 *production of biodiesel*. Catalysis Today, **2015**. 242: p. 3-18.
- 443 19. Komintarachat, C. and S. Chuepeng, *Solid acid catalyst for biodiesel production from waste used*
444 *cooking oils*. Industrial & Engineering Chemistry Research, **2009**. 48(20): p. 9350-9353.
- 445 20. Eze, V.C., A.N. Phan, C. Pirez, A.P. Harvey, A.F. Lee, and K. Wilson, *Heterogeneous catalysis*
446 *in an oscillatory baffled flow reactor*. Catalysis Science & Technology, **2013**. 3(9): p. 2373-
447 2379.
- 448 21. Lee, A.F., J.A. Bennett, J.C. Manayil, and K. Wilson, *Heterogeneous catalysis for sustainable*
449 *biodiesel production via esterification and transesterification*. Chemical Society Reviews, **2014**.
450 43(22): p. 7887-7916.
- 451 22. Sharma, Y.C., B. Singh, and J. Korstad, *Advancements in solid acid catalysts for ecofriendly and*
452 *economically viable synthesis of biodiesel*. Biofuels, Bioproducts and Biorefining, **2011**. 5(1): p.
453 69-92.
- 454 23. Gardy, J., A. Hassanpour, X. Lai, M.H. Ahmed, and M. Rehan, *Biodiesel production from used*
455 *cooking oil using a novel surface functionalised TiO₂ nano-catalyst*. Applied Catalysis B:
456 Environmental, **2017**. 207: p. 297-310.
- 457 24. Sani, Y.M., W.M.A.W. Daud, and A.A. Aziz, *Activity of solid acid catalysts for biodiesel*
458 *production: a critical review*. Applied Catalysis A: General, **2014**. 470: p. 140-161.
- 459 25. Melero, J.A., J. Iglesias, and G. Morales, *Heterogeneous acid catalysts for biodiesel production:*
460 *Current status and future challenges*. Green Chemistry, **2009**. 11(9): p. 1285-1308.
- 461 26. Farabi, M.A., M.L. Ibrahim, U. Rashid, and Y.H. Taufiq-Yap, *Esterification of palm fatty acid*
462 *distillate using sulfonated carbon-based catalyst derived from palm kernel shell and bamboo*.
463 Energy Conversion and Management, **2019**. 181: p. 562-570.
- 464 27. Zhang, J., A. Motta, Y. Gao, M.M. Stalzer, M. Delferro, B. Liu, T.L. Lohr, and T.J. Marks,
465 *Cationic pyridylamido adsorbate on Brønsted acidic sulfated zirconia: A molecular supported*
466 *organohafnium catalyst for olefin homo-and co-polymerization*. ACS Catalysis, **2018**.
- 467 28. Arfaoui, J., A. Ghorbel, C. Petitto, and G. Delahay, *Novel V₂O₅-CeO₂-TiO₂-SO₄²⁻*
468 *nanostructured aerogel catalyst for the low temperature selective catalytic reduction of NO by*
469 *NH₃ in excess O₂*. Applied Catalysis B: Environmental, **2018**. 224: p. 264-275.
- 470 29. Xu, D., X. Lai, W. Guo, X. Zhang, C. Wang, and P. Dai, *Efficient catalytic properties of*
471 *SO₄²⁻/MxOy (M= Cu, Co, Fe) catalysts for hydrogen generation by methanolysis of sodium*
472 *borohydride*. International Journal of Hydrogen Energy, **2018**. 43(13): p. 6594-6602.
- 473 30. Kaur, K., A. Sobti, R.K. Wanchoo, and A.P. Toor, *Studies on glycerol conversion to tricaproin*
474 *over sulfate promoted iron oxide as catalyst using response surface methodology*. Chemical
475 Engineering Research and Design, **2018**.
- 476 31. Li, S., H. Song, Y. Hu, F. Li, and Y. Chen, *A novel method for the synthesis of highly stable*
477 *nickel-modified sulfated zirconia catalysts for n-pentane isomerization*. Catalysis
478 Communications, **2018**. 104: p. 57-61.

- 479 32. Osatiashtiani, A., L.J. Durndell, J.C. Manayil, A.F. Lee, and K. Wilson, *Influence of alkyl chain*
480 *length on sulfated zirconia catalysed batch and continuous esterification of carboxylic acids by*
481 *light alcohols*. Green Chemistry, **2016**. 18(20): p. 5529-5535.
- 482 33. de Almeida, R.M., L.K. Noda, N.S. Goncalves, S.M. Meneghetti, and M.R. Meneghetti,
483 *Transesterification reaction of vegetable oils, using superacid sulfated TiO₂-base catalysts*.
484 Applied Catalysis A: General, **2008**. 347(1): p. 100-105.
- 485 34. Rabee, A.I., G.A. Mekhemer, A. Osatiashtiani, M.A. Isaacs, A.F. Lee, K. Wilson, and M.I. Zaki,
486 *Acidity-reactivity relationships in catalytic esterification over ammonium sulfate-derived*
487 *sulfated zirconia*. Catalysts, **2017**. 7(7): p. 204.
- 488 35. Noda, L.K., R.M. de Almeida, N.S. Gonçalves, L.F.D. Probst, and O. Sala, *TiO₂ with a high*
489 *sulfate content—thermogravimetric analysis, determination of acid sites by infrared*
490 *spectroscopy and catalytic activity*. Catalysis today, **2003**. 85(1): p. 69-74.
- 491 36. Osatiashtiani, A., A.F. Lee, D.R. Brown, J.A. Melero, G. Morales, and K. Wilson, *Bifunctional*
492 *SO₄/ZrO₂ catalysts for 5-hydroxymethylfurfural (5-HMF) production from glucose*. Catalysis
493 Science & Technology, **2014**. 4(2): p. 333-342.
- 494 37. Alhassan, F.H., U. Rashid, and Y. Taufiq-Yap, *Synthesis of waste cooking oil-based biodiesel*
495 *via effectual recyclable bi-functional Fe₂O₃-MnO-SO₄²⁻/ZrO₂ nanoparticle solid catalyst*. Fuel,
496 **2015**. 142: p. 38-45.
- 497 38. Wu, H., Y. Liu, J. Zhang, and G. Li, *In situ reactive extraction of cottonseeds with methyl*
498 *acetate for biodiesel production using magnetic solid acid catalysts*. Bioresource technology,
499 **2014**. 174: p. 182-189.
- 500 39. Guan, D., M. Fan, J. Wang, Y. Zhang, Q. Liu, and X. Jing, *Synthesis and properties of magnetic*
501 *solid superacid: SO₄²⁻/ZrO₂-B₂O₃-Fe₃O₄*. Materials Chemistry and Physics, **2010**. 122(1): p.
502 278-283.
- 503 40. Li, J. and X. Liang, *Magnetic solid acid catalyst for biodiesel synthesis from waste oil*. Energy
504 Conversion and Management, **2017**. 141: p. 126-132.
- 505 41. Zillillah, G. Tan, and Z. Li, *Highly active, stable, and recyclable magnetic nano-size solid acid*
506 *catalysts: efficient esterification of free fatty acid in grease to produce biodiesel*. Green
507 Chemistry, **2012**. 14(11): p. 3077-3086.
- 508 42. Liu, W.-J., K. Tian, H. Jiang, and H.-Q. Yu, *Facile synthesis of highly efficient and recyclable*
509 *magnetic solid acid from biomass waste*. Scientific Reports, **2013**. 3: p. 2419.
- 510 43. Wang, Y.-T., X.-X. Yang, J. Xu, H.-L. Wang, Z.-B. Wang, L. Zhang, S.-L. Wang, and J.-L.
511 Liang, *Biodiesel production from esterification of oleic acid by a sulfonated magnetic solid acid*
512 *catalyst*. Renewable Energy, **2019**. 139: p. 688-695.
- 513 44. Lai, D.-m., L. Deng, Q.-x. Guo, and Y. Fu, *Hydrolysis of biomass by magnetic solid acid*. Energy
514 & Environmental Science, **2011**. 4(9): p. 3552-3557.
- 515 45. Gardy, J., A. Hassanpour, X. Lai, and M.H. Ahmed, *Synthesis of Ti(SO₄)O solid acid nano-*
516 *catalyst and its application for biodiesel production from used cooking oil*. Applied Catalysis A:
517 General, **2016**. 527: p. 81-95.
- 518 46. Roper-Vega, J., A. Aldana-Pérez, R. Gómez, and M. Niño-Gómez, *Sulfated titania*
519 *[TiO₂/SO₄²⁻]: a very active solid acid catalyst for the esterification of free fatty acids with*
520 *ethanol*. Applied Catalysis A: General, **2010**. 379(1-2): p. 24-29.
- 521 47. Shao, G.N., R. Sheikh, A. Hilonga, J.E. Lee, Y.-H. Park, and H.T. Kim, *Biodiesel production by*
522 *sulfated mesoporous titania-silica catalysts synthesized by the sol-gel process from less*
523 *expensive precursors*. Chemical engineering journal, **2013**. 215: p. 600-607.

- 524 48. Tai, Z., M.A. Isaacs, C.M. Parlett, A.F. Lee, and K. Wilson, *High activity magnetic core-*
525 *mesoporous shell sulfonic acid silica nanoparticles for carboxylic acid esterification*. Catalysis
526 Communications, **2017**. 92: p. 56-60.
- 527 49. Saravanan, K., B. Tyagi, R.S. Shukla, and H. Bajaj, *Esterification of palmitic acid with methanol*
528 *over template-assisted mesoporous sulfated zirconia solid acid catalyst*. Applied Catalysis B:
529 Environmental, **2015**. 172: p. 108-115.
- 530 50. Gardy, J.L.I.A., *Biodiesel production from used cooking oil using novel solid acid catalysts*, in
531 *Faculty of Engineering; School of Chemical and Process Engineering 2017*, The University of
532 Leeds Whiterose e-theses, Leeds, UK.
- 533 51. EN-14105, *Fat and oil derivatives. Fatty acid methyl esters (FAME). Determination of free and*
534 *total glycerol and mono-, di-, triglyceride contents*. **2011**. p. 1-26.
- 535 52. Klobes, P., K. Meyer, and R.G. Munro, *Porosity and specific surface area measurements for*
536 *solid materials*. **2006**, National Institute of Standards and Technology: U.S. p. 89.
- 537 53. Yuan, C., H. Liu, and X. Gao, *Magnetically recoverable heterogeneous catalyst: Tungstate*
538 *intercalated Mg–Al-layered double hydroxides-encapsulated Fe₃O₄ nanoparticles for highly*
539 *efficient selective oxidation of sulfides with H₂O₂*. Catalysis letters, **2014**. 144(1): p. 16-21.
- 540 54. Kiss, A.A., F. Omota, A.C. Dimian, and G. Rothenberg, *The heterogeneous advantage: biodiesel*
541 *by catalytic reactive distillation*. Topics in Catalysis, **2006**. 40(1-4): p. 141-150.
- 542 55. Rabee, A.I., L.J. Durndell, N.E. Fouad, L. Frattini, M.A. Isaacs, A.F. Lee, G.A. Mekhemer, V.C.
543 dos Santos, K. Wilson, and M.I. Zaki, *Citrate-mediated sol–gel synthesis of Al-substituted*
544 *sulfated zirconia catalysts for α-pinene isomerization*. Molecular Catalysis, **2018**. 458: p. 206-
545 212.
- 546 56. Xin, T., M. Ma, H. Zhang, J. Gu, S. Wang, M. Liu, and Q. Zhang, *A facile approach for the*
547 *synthesis of magnetic separable Fe₃O₄@TiO₂ core–shell nanocomposites as highly recyclable*
548 *photocatalysts*. Applied Surface Science, **2014**. 288: p. 51-59.
- 549 57. Naeimi, H. and Z.S. Nazifi, *A highly efficient nano-Fe₃O₄ encapsulated-silica particles bearing*
550 *sulfonic acid groups as a solid acid catalyst for synthesis of 1, 8-dioxo-octahydroxanthene*
551 *derivatives*. Journal of Nanoparticle Research, **2013**. 15(11): p. 2026.
- 552 58. Naeimi, H. and S. Mohamadabadi, *Sulfonic acid-functionalized silica-coated magnetic*
553 *nanoparticles as an efficient reusable catalyst for the synthesis of 1-substituted 1 H-tetrazoles*
554 *under solvent-free conditions*. Dalton Transactions, **2014**. 43(34): p. 12967-12973.
- 555 59. Gadamsetti, S., N. Mathangi, S. Hussain, V.K. Velisoju, and K.V. Chary, *Vapor phase*
556 *esterification of levulinic acid catalyzed by γ-Al₂O₃ supported molybdenum phosphate catalysts*.
557 Molecular Catalysis, **2018**.
- 558 60. Sheng, W., W. Wei, J. Li, X. Qi, G. Zuo, Q. Chen, X. Pan, and W. Dong, *Amine-functionalized*
559 *magnetic mesoporous silica nanoparticles for DNA separation*. Applied Surface Science, **2016**.
560 387: p. 1116-1124.
- 561 61. Sen, S., V. Govindarajan, C.J. Pelliccione, J. Wang, D.J. Miller, and E.V. Timofeeva, *Surface*
562 *modification approach to TiO₂ nanofluids with high particle concentration, low viscosity, and*
563 *electrochemical activity*. ACS applied materials & interfaces, **2015**. 7(37): p. 20538-20547.
- 564 62. Wang, J., P. Yang, M. Fan, W. Yu, X. Jing, M. Zhang, and X. Duan, *Preparation and*
565 *characterization of novel magnetic ZrO₂/TiO₂/Fe₃O₄ solid superacid*. Materials letters, **2007**.
566 61(11-12): p. 2235-2238.
- 567 63. Zhao, H., P. Jiang, Y. Dong, M. Huang, and B. Liu, *A high-surface-area mesoporous sulfated*
568 *nano-titania solid superacid catalyst with exposed (101) facets for esterification: facile*
569 *preparation and catalytic performance*. New Journal of Chemistry, **2014**. 38(9): p. 4541-4548.

- 570 64. Vieira, S.S., Z.M. Magriotis, N.A. Santos, A.A. Saczk, C.E. Hori, and P.A. Arroyo, *Biodiesel*
571 *production by free fatty acid esterification using lanthanum (La^{3+}) and HZSM-5 based catalysts.*
572 *Bioresource technology*, **2013**. 133: p. 248-255.
- 573 65. Jamil, F., H. Ala'a, M.T.Z. Myint, M. Al-Hinai, L. Al-Haj, M. Baawain, M. Al-Abri, G. Kumar,
574 and A. Atabani, *Biodiesel production by valorizing waste Phoenix dactylifera L. Kernel oil in the*
575 *presence of synthesized heterogeneous metallic oxide catalyst ($Mn@ MgO-ZrO_2$).* *Energy*
576 *Conversion and Management*, **2018**. 155: p. 128-137.
- 577 66. Zhang, Z., H. Huang, X. Ma, G. Li, Y. Wang, G. Sun, Y. Teng, R. Yan, N. Zhang, and A. Li,
578 *Production of diacylglycerols by esterification of oleic acid with glycerol catalyzed by diatomite*
579 *loaded SO_4^{2-}/TiO_2 .* *Journal of industrial and engineering chemistry*, **2017**. 53: p. 307-316.
- 580